A CEFI-based Magnetic Resonance Coupling Wireless Power Transfer System for Increased Power Output

Arshaque Ali, *Grad. Member, IEEE*, and Utkal Mehta, *Sr. Member, IEEE*.

***Abstract*—This paper presents a novel approach to magnetic resonance coupling wireless power transfer (WPT). The proposed design implements a capacitive element with a fractional impedance (CEFI) of the order of less than unity in the receiving circuit. Existing research has primarily explored fractional-orders greater than one. However, experimental results demonstrate significant benefits from sub-unity fractional elements. Mathematical analysis and experimental validation of a series-series compensated system show promising results. With a CEFI of the order of 0.98, the system achieves a 169% increase in DC power output and a 137% improvement in AC power output compared to a similar classical system. The design maintains DC-DC efficiency and experiences only a 5% reduction in AC-AC efficiency at high coupling coefficients. These findings establish sub-unity fractional impedance components as viable solutions for WPT performance improvement.**

***Index Terms*—Wireless Power Transfer (WPT), Magnetic Resonance Coupling (MRC), Fractional-Order Capacitor, Series-Series (S-S) Compensation, Power Optimisation, Load Matching, Fractional-Order Element, Air-Core Coils, Impedance Matching.**

I. Introduction

Wireless power transfer (WPT) has become a foundational technology for diverse applications, including biomedical implants, consumer electronics, and electric vehicle (EV) charging. Among the available techniques, Magnetic Resonance Coupling (MRC) offers high efficiency at mid-range distances and reduced alignment sensitivity, making it one of the most promising approaches [1], [2]. However, practical MRC-WPT systems often encounter limitations such as narrow bandwidth, reduced performance under misalignment, and limited adaptability to variable load conditions.

Recent investigations have explored the integration of fractional-order elements (FOEs), also known as elements with fractional impedance (EFIs), into WPT systems to enhance performance and design flexibility [3]–[6]. These elements generalise the behaviour of conventional capacitors and inductors by introducing a non-integer order relationship between voltage and current, enabling improved control over resonance characteristics and impedance matching. Despite these advantages, most studies have concentrated on active or complex realisations with fractional-orders $\alpha > 1$, which are challenging to implement and often unsuitable for compact or passive designs.

In contrast, capacitive elements exhibiting fractional-order behaviour with $0 < \alpha < 1$ offer a promising alternative. These passive components, often realised through nanoporous dielectrics or constant-phase elements, can be more easily integrated into practical systems without the need for active control circuitry [7], [8]. However, the influence of such elements on key performance metrics in MRC-WPT systems, such as voltage gain, efficiency, and power delivery, remains insufficiently explored.

This paper addresses this gap by analysing a resonant WPT topology that incorporates a passive capacitive element with fractional impedance (CEFI) into the receiver-side compensation network. A comprehensive theoretical model is developed to evaluate the system's voltages, currents, impedance profiles , power transfer, and efficiency across a range of coupling coefficients and load conditions. The analysis is supported by circuit simulations and experimental measurements, confirming the validity of the proposed approach.

The specific contributions of this work are as follows:

- A resonant WPT architecture is proposed that includes a passive CEFI with fractional-order $\alpha < 1$ in the receiver compensation branch.
- Closed-form analytical expressions are derived for voltages, currents, efficiency, and power transfer, incorporating the effects of fractional-order impedance.
- Time-domain simulations and hardware experiments are conducted to validate the model and quantify performance across varying coupling strengths and loads.
- The trade-offs introduced by FOEs are discussed, including observed improvements in alternating current (AC) performance and robustness at the expense of slight reductions in direct current (DC) efficiency.

The layout of this paper is organised as follows. Section II provides a review of the existing literature on the application of fractional-order components in wireless power transfer systems. Section III details the system modelling and analytical derivations, followed by numerical simulations and circuit-level validation. Section IV outlines the experimental setup and implementation methodology, leading into Section V, which presents and analyses the measured results to evaluate the effectiveness of the proposed design. Section VI then explores key design considerations and performance trade-offs observed

A. Ali and U. Mehta are with the Electrical and Electronics Engineering at the University of the South Pacific, Fiji Islands. (e-mails: tiazyroz@gmail.com, utkal.mehta@usp.ac.fj).

during experimentation. Finally, Section VII concludes the paper and outlines directions for future research.

II. Related Works

Fractional calculus provides a generalisation of classical differentiation and integration, enabling the modelling of dynamic systems that exhibit memory and hereditary properties [9]. In the electrical domain, FOEs exhibit impedance characteristics that are neither purely capacitive nor inductive and instead follow a power-law frequency response of the form $Z(s) \propto s^{\alpha}$, where α is the fractional-order. FOEs with $0 < \alpha < 1$ behave as passive elements, while those with $\alpha > 1$ may introduce active characteristics and potential instability [10], [11]. Early experimental work on the application of FOEs to WPT systems demonstrated that such elements could offer improved performance in scenarios that involve detuning or varying load conditions. For example, [4] integrated a high-power CEFI of fractional-order $\alpha = 1.013$ on the receiver side of an S-S MRC-WPT topology. The system exhibited enhanced stability and reduced sensitivity to receiver-side parameter drift, achieving efficient energy transfer without requiring real-time feedback or adaptive tuning mechanisms. Similarly, in [3], the authors employed a CEFI with $\alpha = 1.015$ at the transmitter of a 30 W, 200 kHz MRC system. This configuration achieved a regulation of the output voltage within ± 0.6 V and maintained an efficiency above 92.7% over a range of coupling coefficients ($k = 0.1$ to $k = 0.2$), demonstrating that fractional capacitors with $\alpha > 1$ can improve tolerance to misalignment. However, such systems often rely on active elements or synthesised circuits that incorporate negative impedance converters, which can be complex to implement and may introduce stability and control challenges. In contrast, more recent work has begun to explore FOEs with $\alpha < 1$, which remain strictly passive and are more suitable for hardware realisation using ladder networks, constant phase elements (CPEs), or dielectric composites. For example, [12] investigated the use of a fractional capacitor on the receiver side of a loosely coupled system and reported a 29 fold increase in load voltage compared to a baseline case. However, the system's maximum power transfer efficiency remained relatively low (21.4%), highlighting the trade-off between voltage gain and overall energy efficiency. In [2], a passive CEFI with order $\alpha = 0.54$ was designed using network synthesis techniques and deployed in a resonant converter. The results showed that the operating frequency of the system could be reduced while maintaining the same power level, owing to the FOE's enhanced energy storage capabilities at lower frequencies. Although promising, the work lacked a direct comparison to classical systems and did not extend to physical prototype validation.

The work in [5] examined both S-S and S-P topologies incorporating FOEs with fractional-order $\alpha = 0.9$. The analysis showed that the FOE-based circuits offered smoother efficiency profiles over a range of load resistances and coupling coefficients. While the peak efficiency of the fractional system was lower than that of its classical counterpart, the increased flexibility and tuning range made it attractive for dynamically changing environments. This trade-off between adaptability and peak efficiency remains a recurring theme in the fractional-order WPT literature. Some practical challenges to handling issues in WPT have recently been discussed. In electric vehicles, constant current and voltage are required. A compact WPT design was proposed in [13] using the S-S compensation topology. One known issue in WPT is parameter perturbation within the WPT resonant network. It was rectified in [14] using a switch-controlled capacitor with a control angle calibrated during a system self-check process before high-power charging. Another reliable power circuit was presented using an 8-coil multinode WPT transmission network, developed by Wang et al. [15]. This scheme was realized with composite insulators and a single load coil. In this way, one can see some huge potential in conducting research in WPT-related applications.

A summary of these systems together with the proposed system is provided in Table I, highlighting key parameters such as topology, frequency, power rating, fractional-order, and performance results. Across the literature, it is observed that systems employing FOEs with $\alpha > 1$ often achieve higher efficiency and robustness but rely on active or synthetic components. Conversely, systems with $\alpha < 1$ tend to be passive and simpler to realise in hardware, yet require more rigorous analysis to quantify their performance and identify optimal operating conditions.

An additional challenge in the literature is the mathematical modelling of fractional-order WPT systems. While several works adopt complex formulations involving fractional Laplace transforms, convolution integrals, or sigmoid-based impedance shaping to avoid negative resistance, such techniques are not necessary when designing for $\alpha < 1$. In this regime, impedance remains strictly positive and bounded, making the system more amenable to classical circuit analysis techniques. Nevertheless, simplified and closed-form expressions for output power and efficiency in such systems are rarely presented, limiting the practical adoption of FOEs in MRC-WPT designs.

To date, few studies offer full-wave simulation or experimental validation of fractional-order systems using passive capacitive FOEs. Moreover, there remains a gap in the literature regarding the derivation of analytical expressions tailored for such systems, particularly in DC-DC applications where input-output efficiency metrics are critical. This motivates further investigation into the behaviour, modelling, and implementation of MRC-WPT systems incorporating passive CEFIs with $\alpha < 1$, which form the basis for the present work.

III. Theoretical Modelling and Simulations

To understand and quantify the influence of CEFIs on the performance of MRC-WPT systems, a comprehensive analytical model is developed in this section. The model is based on an impedance matrix representation of the coupled system, allowing for the derivation of closed-form expressions for key performance metrics such as input and output impedance, voltages, currents and power transfer efficiency. These theoretical insights are then validated through numerical simulations,

TABLE I
KEY DETAILS OF REALIZED WORKS

Reference	Operating Frequency	Inverter Type	Topology	α	Efficiency	Key Novelty
[3]	210.97 to 208.33 kHz	Full-Bridge	S-S	>1	92.7%	- Achieves constant current or constant voltage charging - High misalignment tolerance - Adaptive natural resonant frequency
[4]	491.6 kHz	Half-Bridge	S-S	>1	$>$90%	- Insensitive to variations in receiver's resonant frequency
[16]	50 kHz	Half-Bridge	S-S	>1	$>$90%	- Achieves inherently constant current output - Appropriate parameters chosen for fractional-order capacitor - No communication or control between transmitter and receiver
[17]	178.5 kHz	Not specified	S-S	>1	$>$35%	- Uses fractional-order components - Proposes coupled-mode theory for fWPT - Greater design freedom - Better dynamic characteristics
[2]	520 kHz	Class-E	S-S	<1	-	- CEFI and IEFI used - Reduces operating frequency - Improves power quality
This work	125 kHz	Full-Bridge	S-S	<1	$>$78%	- Passive CEFI implementation - $\alpha < 1$ - Comparison with cWPT - Simplified fractional model - Experimental validation - Analysis of power-efficiency trade-offs

which highlight the role of α in system performance across various coupling coefficients and load conditions.

A. Impedance Matrix Representation

Considering the coupling components of the transmission and receiving circuits as a two-port network, the impedance matrix (Z) can easily be derived for any coupled inductive or capacitive WPT system. The Z matrix is formed by the resistive and reactive counterparts when measured across or at the two ports in four different configurations. This matrix can be expressed as a combination of two other matrices, as shown in (1).

$$\begin{bmatrix} Z_{11} & Z_{12} \\ Z_{21} & Z_{22} \end{bmatrix} = \begin{bmatrix} R_{11} & R_{12} \\ R_{21} & R_{22} \end{bmatrix} + j \begin{bmatrix} X_{11} & X_{12} \\ X_{21} & X_{22} \end{bmatrix} \tag{1}$$

In the resistance matrix (R), R_{11} represents the resistance seen at port 1 when port 2 is open, R_{12} represents the transfer resistance from port 2 to port 1, R_{21} represents the transfer resistance from port 1 to port 2, and S_{22} represents the resistance seen at port 2 when port 1 is open. Similarly, for the reactance matrix (X), X_{11} represents the reactance seen in port 1 when port 2 is open, X_{12} represents the transfer reactance from port 2 to port 1, X_{21} represents the transfer reactance from port 1 to port 2, and X_{22} represents the reactance seen at port 2 when port 1 is open. j is the imaginary unit that has the value of $\sqrt{-1}$. In a reciprocal network, $R_{12} = R_{21}$ and $X_{12} = X_{21}$, which is often the case for symmetric passive networks. For the S-S compensation topology, the matrices R and X can be defined using fractional calculus according to (2). Note that these equations consider the series connection of the capacitor in both the transmission and reception circuits and incorporate fractional impedance characteristics in the analysis.

$$\begin{aligned} R_{11} &= \frac{1}{\omega^{\alpha_1} C_1} \cos\frac{\alpha_1 \pi}{2} + \omega^{\beta_1} L_1 \cos\frac{\beta_1 \pi}{2}, \\ R_{12} &= R_{21} = \omega^{\gamma} M_{\gamma} \cos\frac{\gamma \pi}{2}, \\ R_{22} &= \frac{1}{\omega^{\alpha_2} C_2} \cos\frac{\alpha_2 \pi}{2} + \omega^{\beta_2} L_2 \cos\frac{\beta_2 \pi}{2} \end{aligned} \tag{2}$$

$$\begin{aligned} X_{11} &= \frac{1}{\omega^{\alpha_1} C_1} \cos\frac{\alpha_1 \pi}{2} + \omega^{\beta_1} L_1 \cos\frac{\beta_1 \pi}{2}, \\ X_{12} &= X_{21} = \omega^{\gamma} M_{\gamma} \sin\frac{\gamma \pi}{2}, \\ X_{22} &= \frac{1}{\omega^{\alpha_2} C_2} \sin\frac{\alpha_2 \pi}{2} + \omega^{\beta_2} L_2 \cos\frac{\beta_2 \pi}{2} \end{aligned} \tag{3}$$

where,

- α_1 and α_2 represent the fractional-order of the transmission and reception compensation capacitors, respectively.
- β_1 and β_2 represent the fractional-order of the transmission and reception coils, respectively.
- C_1 and C_2 represent the conventional capacitance of the transmission and reception compensation capacitors, respectively.

- L_1 and L_2 represent the conventional inductance of the transmission and reception coils, respectively.
- ω is the angular operating frequency given by $\omega = 2\pi f$.
- γ is the fractional-order of the mutual inductance.
- M is the equivalent mutual impedance given by $M = k\sqrt{L_1 L_2}$.

Using (2) and (3), one can also present the impedances of the transmission circuit, the mutual inductance, and the reception circuit as (4).

$$\begin{bmatrix} Z_{\text{in}} \\ Z_{MI} \\ Z_{\text{out}} \end{bmatrix} = \begin{bmatrix} Z_{11} \\ Z_{12} \\ Z_{22} + Z_{load} \end{bmatrix} = \begin{bmatrix} R_{11} + j(X_{11}) \\ R_{12} + j(X_{12}) \\ R_{22} + R_{load} + j(X_{22} + X_{load}) \end{bmatrix} \tag{4}$$

(1) - (4) are useful to perform the analysis and compute the optimised parameters for any dual antenna-based coupled S-S compensated system.

B. Efficiency and Load Optimisation

The parameter k represents the coupling strength between two coils. It is a value between 0 and 1. A low value is representative of a large transfer distance and/or misalignment, whereas a value closer to 1 represents an ideally coupled scenario. In practice, it is very difficult to obtain a coupling coefficient value close to 1 as a result of the coils being air-coupled, which inherently introduces losses into the system. This is one of the main factors that explains why large transfer distances have poor efficiencies. However, with the experimental setup developed at MIT, 60 W of power was transmitted over a distance of 2 m [1]. This led to speculation that there could be other factors to optimise to achieve a large transfer distance with acceptable efficiency levels. In the following, the kQ relationship has been represented for any generalised two-port network [18],

$$kQ = \sqrt{\frac{R_{11}R_{22} - R_{12}R_{21}}{R_{11}R_{22} + X_{12}X_{21}} - 1}, \tag{5}$$

as a single figure of merit. This relationship enables the calculation of the kQ product while allowing one to consider parasitic resistances and fractional characteristics of the system. It is worth mentioning that when all fractional-orders are set to unity, i.e. $\alpha, \beta, \gamma = 1$, the equations take the form of classical integer-order relationships. In the above equation, Q, which represents coil quality, is a key factor when it comes to increasing the practical efficiency of a WPT system. This Q is a measure of the distance the inductor is from an ideal one and expresses its suitability to be used at high frequencies. It is calculated using (6) where the R term is the resistance measured at f.

$$Q = \frac{X_L}{R} = \frac{2\pi f \mu r \mu_0 N^2 \pi r^2}{LR} \tag{6}$$

The equation (6) highlights the relationship between the various specifications of a coil (such as length, resistance, number of turns, and radius) and the coil quality. The factor Q preferably needs to be of a large value, and the equation implies that a large inductive reactance is suitable for this. To increase the inductive reactance, one could increase the inductance value or the operating frequency. These increases would then affect the length of the coil and the resistance, negatively impacting Q. Therefore, it is important to find a balance between these parameters to achieve a high Q and maximum efficiency.

The maximum achievable efficiency is dependent on the compensation topology of the network and the inherent characteristics of the coils and capacitors themselves. Using (2) and (3), the maximum achievable frequency is expressed as (7). This equation is useful for directly calculating efficiency using the input, output, and mutual impedance components of the transmission and reception circuits.

$$\eta_{max} = \frac{\sqrt{(R_{11}R_{22} + X_{12}X_{21})} - \sqrt{(R_{11}R_{22} - R_{12}R_{21})}}{\sqrt{(R_{11}R_{22} + X_{12}X_{21})} + \sqrt{(R_{11}R_{22} - R_{12}R_{21})}} \tag{7}$$

The optimal load impedance, Z_{opt} is calculated as a complex combination of resistance and reactance that achieves the maximum power transfer efficiency given by (7). The equation for Z_{opt} is,

$$\begin{aligned} Z_{opt} = {} & \frac{\sqrt{(R_{11}R_{22} - R_{12}R_{21})(R_{11}R_{22} + X_{12}X_{21})}}{R_{11}} \\ & + j\left(\frac{R_{21}X_{21}}{R_{11}} - X_{22}\right) \end{aligned} \tag{8}$$

C. Simulation Results

To validate the theoretical framework and quantify the impact of incorporating fractional capacitive elements, numerical simulations were conducted using MATLAB©. The analytical models were built using the impedance expressions developed in (1) - (4), with system parameters listed in Table II. The inductance and resistance values were measured using an LCR metre at 100 kHz, the closest available frequency to the system target operating frequency of 125 kHz. The choice of 125 kHz as the operating frequency is based on the coil specifications, which exhibit a high Q at this frequency, making it the optimal point for efficient operation. Although there are slight impedance differences between 100 and 125 kHz, they are not significant enough to affect the overall analysis.

TABLE II
SIMULATION CIRCUIT PARAMETERS

Parameter	Value
V_s	10 V_{RMS}
f_o	125 kHz
R_{p1}	0.1346Ω
R_{p2}	0.1231Ω
L_1	10.760 μH
L_2	10.616 μH

The three-dimensional surface plot in Figure 1 shows the relationship between the efficiency of the system η and R_L and α_2. The mapping reveals that optimal performance, approximately 85%, is achieved with low load resistance values in the range of 0.5-10 Ω with α_2 approaching unity.

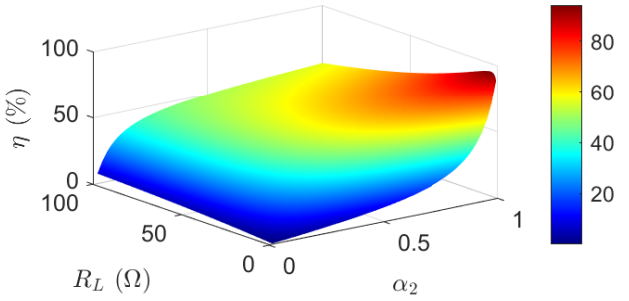

Fig. 1. The variation of maximum efficiency with respect to changes in R_L and α_2 with $k = 0.5$

The transition from blue to red demonstrates how η is sensitive to α_2. The upper right region indicates a steep efficiency gradient, suggesting that small deviations in R_L or α_2 in this region affect system performance. Referring to (8), it becomes obvious Z_{opt} varies with k. Figure 2 helps to visualise how much the Z_{opt} changes with k. η shows a strong correlation with both parameters and transitions, from lowest to highest. The system achieves optimal performance with higher k combined with relatively low R_L. This performance landscape shows rapid η changes in the range of $k < 0.3$, as indicated by the steep gradient in the blue-to-green region. As k increases, the system becomes more stable and less sensitive to variations in R_L while maintaining high levels of η. The smooth surface progression of the plot reveals that stronger magnetic coupling between the TX and RX coils, along with appropriate load matching, is key to achieving maximum η. Table III contains data on how the Z_{opt} shifts as α_2 is reduced from the ideal scenario of $\alpha_2 = 1$.

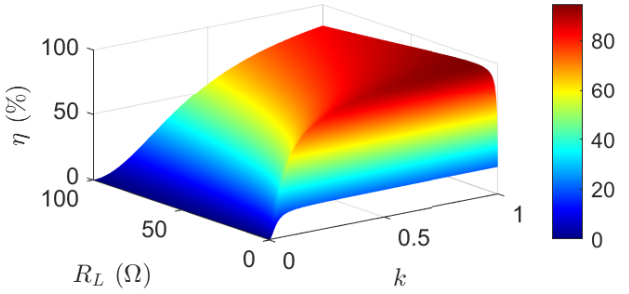

Fig. 2. The variation of optimum load for maximum efficiency at various coupling coefficients.

These results show the differences between the Z_{opt} of each k when the fractional nature is considered. It is observed that as α_2 is reduced from the ideal case, Z_{opt} increases, which is a desirable characteristic. For all k, with α_2 set to 0.97, Z_{opt} is seen to increase in magnitude by two-fold i.e., for $k = 0.5$, R_L changes from 4 Ω to 8.2 Ω. The load optimisation should also be done based on the k it will be engaged with; in practical scenarios, the TX and RX coils have to be near to achieve a high k [19]. The η plot for k and α_2 shown in Figure 3 reveals a gradual but consistent improvement in η as both

TABLE III
MAXIMUM LOAD RESISTANCE (Ω) FOR VARIOUS k AND α_2 VALUES

k \ α_2	1	0.99	0.98	0.97
0.1	0.8008	1.2012	1.5015	1.7017
0.3	2.4024	3.5035	4.3043	5.005
0.5	4.0040	5.8058	7.1071	8.2082
0.7	5.6056	8.1081	9.9099	11.512
0.9	7.2072	10.4100	12.8130	14.8150

parameters increase, with the steepest η gradients occurring in the outer values, shown by the region in orange and red. This visualisation effectively shows how the fractional-order parameter can be used in conjunction with the k to optimise system performance, although the highest η are ultimately achieved with ideal capacitors and strong coupling.

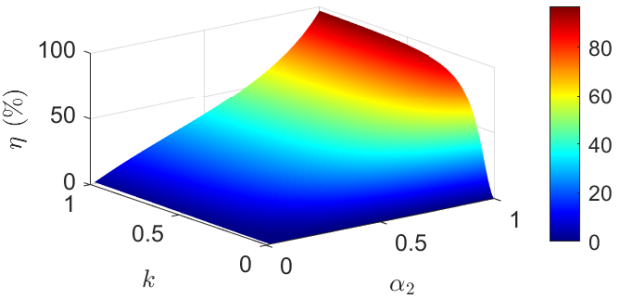

Fig. 3. The variation of maximum achievable efficiency for coupling coefficient for various fractional-orders

Using the same parameters from Table II, with the addition of $R_L = 5\Omega$, the system was simulated for three coupling values ($k = 0.2, 0.6, 0.8$). R_L is selected as 5 Ω, as it falls within the optimal efficiency range for both cWPT and fWPT systems, achieving around 85% efficiency when the fractional parameter α_2 approaches unity. Extending (1)-(4) to obtain relationships for currents, voltages, power, and efficiency gives rise to the following:

$$I_1 = \frac{V_s Z_{22}}{\xi} \tag{9}$$

$$I_2 = -\frac{V_s Z M}{\xi} \tag{10}$$

$$\xi = Z_{11} Z_{22} - Z_M^2 \tag{11}$$

$$V_{out} = |I_2| R_L \tag{12}$$

$$P_{in} = V_{in} |I_1| \tag{13}$$

$$P_{out} = |I_2|^2 R_L \tag{14}$$

$$\eta = \frac{P_{out}}{P_{in}} \times 100 \tag{15}$$

The above explicit expressions of voltage, current, power, and efficiency can allow a direct comparison of the values with those acquired from circuit simulation. The simulation schematic is shown in Figure 4, where the switch position 'A' forms the cWPT and 'B' forms the fWPT. Tables IV and V

TABLE IV
CWPT - COMPARISON OF CALCULATED AND SIMULATED RESULTS

Parameter	$k = 0.2$		$k = 0.6$		$k = 0.8$	
	C_P	C_{SIM}	C_P	C_{SIM}	C_P	C_{SIM}
$\|I_1\|$ (A)	14.4726	14.32	1.9448	1.938	1.1066	1.103
$\|I_2\|$ (A)	4.7640	4.744	1.9206	1.927	1.4571	1.462
V_{out} (V)	23.8200	23.72	9.6028	9.634	7.2855	7.312
P_{in} (W)	144.7257	143.2	19.4482	19.38	11.0664	11.03
P_{out} (W)	113.4782	112.5	18.4426	18.56	10.6157	10.69
η (%)	78.4091	78.59	94.8295	95.78	95.9281	96.93

TABLE V
FWPT - COMPARISON OF CALCULATED AND SIMULATED RESULTS

Parameter	$k = 0.2$		$k = 0.6$		$k = 0.8$	
	C_P	C_{SIM}	C_P	C_{SIM}	C_P	C_{SIM}
$\|I_1\|$ (A)	15.0693	14.96	2.0426	2.036	1.1630	1.159
$\|I_2\|$ (A)	4.7165	4.716	1.9180	1.925	1.4560	1.462
V_{out} (V)	23.5824	23.58	9.5898	9.627	7.2799	7.309
P_{in} (W)	150.6931	149.6	20.4265	20.36	11.6298	11.59
P_{out} (W)	111.2255	111.2	18.3928	18.53	10.5994	10.68
η (%)	73.8093	74.34	90.0439	91.05	91.1401	92.17

show the calculated values using (9) - (15) and the simulation measurements in a side-by-side format.

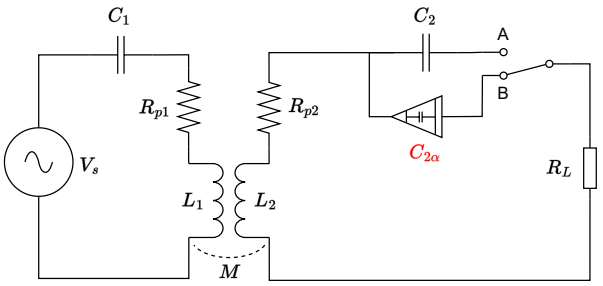

Fig. 4. Fractional order capacitor in WPT circuit.

The calculated values appear in columns labelled C_P, while the circuit simulation results are listed in columns labelled C_{SIM}. The listed data include the magnitude of primary and secondary currents, $|I_1|$ and $|I_2|$, output voltage, V_{out}, input power, P_{in}, output power, P_{out}, and efficiency, η. The η in this section represents the AC-AC efficiency maintaining consistency with the analytical model. This ensures that the experimental results and the theoretical calculations are on the same footing for an accurate comparison.

For each k, the calculated values show close agreement with the simulated results, showing only minor discrepancies. This alignment is notable in power and efficiency measurements, where the calculated efficiencies almost match the simulated values, especially at higher coupling coefficients, indicating improved model accuracy with stronger coupling. The strong correlation between C_P and C_{SIM} in all parameters validates the accuracy of the analytical model to capture the performance of the WPT system under varying coupling conditions.

The results of numerical and circuit simulations show that neglecting fractional characteristics can lead to flawed optimisations, especially in extreme cases. While some manufacturers produce near-ideal capacitors with orders close to 1, these components are costly and require system identification to verify their actual order. This process is complex due to challenges in distinguishing true fractional behaviour from other non-ideal effects, requiring precise measurements over a wide frequency range. Accurate modelling and validation under different conditions add to the difficulty. An alternative for achieving predictable fractional behaviour is designing CEFIs using network synthesis to approximate fractional impedance characteristics.

IV. PRACTICAL IMPLEMENTATION OF PROPOSED FRACTIONAL WPT SYSTEM

To translate the theoretical model into a practical system, a hardware prototype of the fWPT system was developed. The implementation integrates a high-frequency inverter, magnetically coupled coils, and a synthesised CEFI integrated on the receiver side. The design follows the S-S compensation topology and operates at a resonant frequency of 125 kHz. The experimental setup was developed to test both the cWPT and fWPT configurations under identical conditions for performance comparison. A block diagram of the system is shown in Figure 5.

A. Coil Selection and Design

The selection of coils is critical to achieving high transfer efficiency in MRC-based WPT systems as their characteristics govern system operation. The operating frequency or *resonant frequency,* f significantly influences the performance of the system as it involves resonating the coils at a specific frequency to achieve efficient energy transfer between the coils. In MRC-based systems, a compensation capacitor is used with the transmitting and receiving coils to tune the units to operate at the desired f.

The secondary but core parameter of a WPT coil is the quality factor, Q. This provides a measure of the efficiency and effectiveness of energy storage and transfer. A higher value Q indicates that the coil has lower energy losses, as it can sustain oscillations for an extended period, leading to improved power transfer efficiency and longer transfer distance [1]. A high value also implies a coil's ability to operate at high frequencies. The selection of the operating resonance frequency for an MRC-based WPT system is greatly aided by referring to this parameter. The coil quality does not have a specific range; however, it depends on the resistance and reactance of the coil at the rated frequency. According to [20], air core coils with ferrite plates typically have a Q between 100 and 300 and can be calculated using (6).

In the proposed work, we have used WE-WPCC wireless power transfer coils manufactured by Wurth Elektronik, shown in Figure 6 due to their high Q, ferrite backing and compact form factor. The coil specifications are summarised in Table VI and were used in both the simulation and hardware implementation.

B. High-Frequency Transmitter Design

Designing a high-frequency inverter can be challenging, particularly when variable-frequency operation is required.

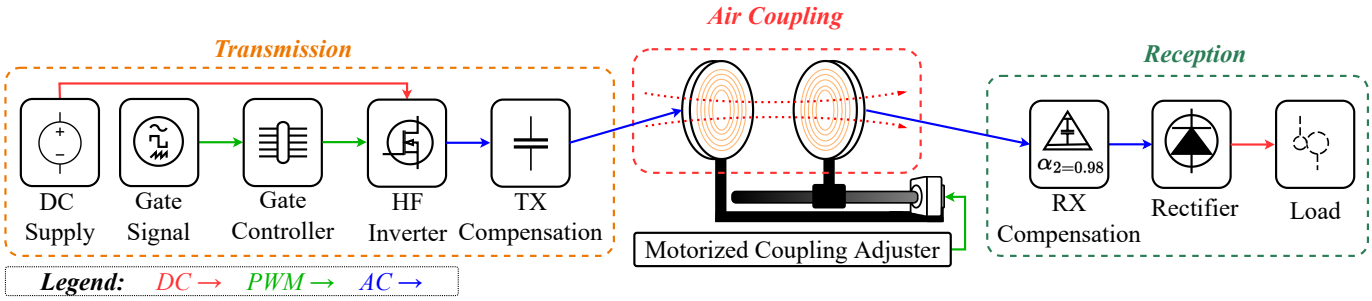

Fig. 5. Block diagram of proposed fWPT system

Fig. 6. WE-WPCC (760308100141) wireless power transfer coil.

TABLE VI
COIL SPECIFICATIONS

Properties	Value	Test Condition
Inductance	10.5 μH	10 mA, 125 kHz
Q - factor	180	10 mA, 125 kHz
Rated Current	9A (max)	$\Delta T = 40K$
DC Resistance	30 mΩ	$20°C$
SRF	11 MHz	

These challenges arise from the efficient generation and control of high-frequency AC signals while maintaining stable performance. The proposed topology employs a combination of two IR2184 half-bridge drivers, which are high-speed MOSFET and IGBT-compatible ICs with integrated bootstrapping. Bootstrapping is a technique used to provide a floating voltage supply to the high-side gate driver in a half-bridge or full-bridge topology. It involves the use of a capacitor to capture a portion of the gate drive signal and use it to create a voltage level higher than the supply voltage, allowing the gate driver to effectively turn on and off the high-side switching device. This is important for high-frequency inverter designs, where gate drive requirements are more demanding. The control signals for the four MOSFETs are generated internally by the IC and only require a single switching signal at the resonant frequency at each of the respective IC pins. This switching signal is generated by an Arduino Nano, configured to output an adjustable PWM frequency using a potentiometer.

C. Realization of the CEFI via Network Synthesis

The design of CEFIs involves various mathematical methods to approximate fractional-order impedance characteristics to allow practical realisations of these elements in circuit applications. The Continued Fractional Expansion (CFE) representation consists of a sequence of terms, each term being a fraction with a numerator and a denominator. The numerator can be a constant or a variable, while the denominator is typically a sum of a constant and a variable multiplied by the previous term's denominator. The continued fraction representation is expressed using square brackets and can be written as (16).

$$a_0 + \cfrac{b_1}{a_1 + \cfrac{b_2}{a_2 + \cfrac{b_3}{a_3 + \cfrac{b_4}{a_4 + \dots}}}} \tag{16}$$

Here a_0 is the whole number part, and the subsequent pairs (a_1, b_1), (a_2, b_2), (a_3, b_3) are the numerators and denominators of the nested fractions. CFE offers a concise representation of real numbers and has various applications in mathematics, physics, and engineering. It can approximate irrational numbers, calculate continued fractions of functions, solve certain equations, and analyse the behaviour of systems with fractional-order components. In the fractional-order approximation of components like capacitors or inductors, CFE is employed to rationalise the fractional-order transfer function and realise the impedance using specific forms of network synthesis. The impedance of a fractional-order capacitor is ideally expressed by (17).

$$Z_C(s) = \frac{1}{C_\alpha s^\alpha} \tag{17}$$

where, C_α and α represent the pseudocapacitance and fractional-order of the CEFI and respectively. The pseudocapacitance can be expressed as a function of conventional capacitance as shown in (18), where f is the resonant frequency is in Hz. C, the conventional capacitance is a measurable parameter and synonymous with the capacitance of classical capacitors.

$$C = \frac{C_\alpha}{(2\pi f)^{1-\alpha}} \tag{18}$$

By expressing (17) as a calculated parameter from (1) - (4), four network approximation techniques can be used to synthesise the CEFI, namely, Cauer I, Cauer II, Foster I, and Foster II. The Cauer and Foster I forms use impedance functions directly, while Foster II requires the admittance representation. Cauer networks, developed by Wilhelm Cauer, use ladder structures of resistors, capacitors, and inductors to approximate impedance functions. The Cauer I form, known

as the $z-$ form, alternates series-connected resistors with parallel-connected capacitors in a ladder structure, as shown in Figures 7 and 8. This configuration effectively approximates high-order impedance functions while using fewer components than other forms. This work implements the Cauer I network due to its superior approximation accuracy compared to other forms.

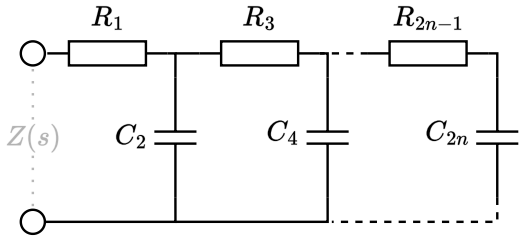

Fig. 7. Cauer I network structure

A detailed explanation of such approximations can be found in [21]. A prior study demonstrated that sub-unity constant equivalent fractional impedances perform better when the fractional-order is close to 1 [22]. Simulations across fractional-orders from 0.1 to 0.9 revealed that orders close to 1 yielded high efficiency, while lower orders led to poor performance due to inadequate circuit tuning. Similarly, the numerical and simulation results from subsection III-C also highlight the same point. These findings justify focusing on higher fractional-orders for optimal performance. Using (17) and circuit parameters listed in Table II, the resistor and capacitor values used for the CEFI approximation with $\alpha_2 = 0.98$ are provided in Table VII. These values are computed using a modified version of [23], which derives the pseudocapacitance value using the impedance components of the fWPT system. The fractional-order has been verified by measuring the phase shift between the input voltage and current to the CEFI using (19).

$$\alpha = \frac{\phi}{-90^{\circ}} \tag{19}$$

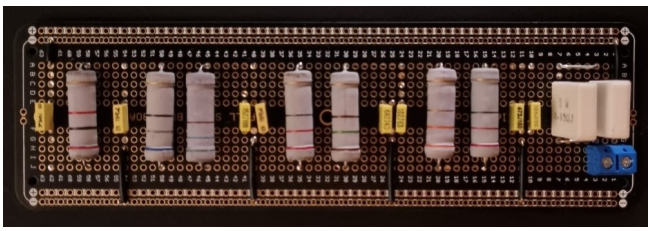

Fig. 8. Cauer I Realized CEFI

To note, R_p is the resistor connected in parallel to the network (Figure 8) to achieve a corrected impedance response.

D. Motorised Coupling Adjuster

The precise control of mutual coupling between the transmitter and receiver coils necessitated the implementation of a high-precision linear actuator system, capable of achieving positional accuracy within $\pm$ 0.6 mm. The mechanical assembly comprises a fixed TX coil mounted to the actuator housing, while the RX coil is fixed to the movable slide block. To ensure mechanical stability and electrical isolation, both coils are secured to 5 mm thick acrylic mounting plates prior to their integration with the linear actuator assembly, as shown in Figure 9.

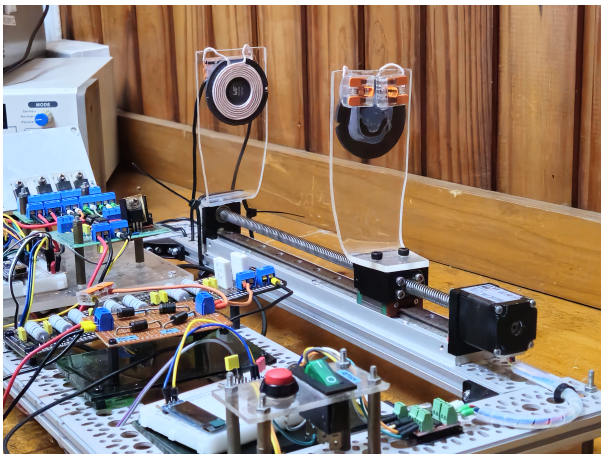

Fig. 9. TX and RX coils mounted to linear actuator

The linear motion mechanism is driven by a NEMA 11 stepper motor, which interfaces with an Arduino Nano microcontroller through a dedicated motor driver circuit. The control system incorporates two user interface elements: a bidirectional toggle switch for selecting the direction of RX coil movement (either increasing or decreasing the transfer distance) and a push-button interface that triggers discrete positional increments of 0.6 mm in the selected direction.

E. Test Environment and Instrumentation

The experimental validation system is depicted in Figure 10, and its key electrical parameters are listed in Table II. The setup also used a 5 Ω aluminium-housed load resistor, chosen based on the load optimisation results to ensure consistency and comparability with the simulation studies. To enable precise control over k, the distance between the transmitter and receiver coils was increased or decreased using the motorised coupling adjuster.

This approach ensured consistent spacing and facilitated reliable calculation of k based on separation distance. Due to the inherent sensitivity of k to alignment and coil geometry and the practical difficulty of measuring it directly with high accuracy, this study defines the relationship between coupling coefficient and physical distance using representative ranges, as shown in Table VIII. This approach accounts for practical uncertainties and variabilities in coil positioning. Two sets of data were collected to evaluate and compare system efficiency in both domains: (1) η_{AC-AC}, voltage and current were measured at the output of the high-frequency inverter (TX side) and directly at the receiver coil (RX side), with the full-bridge rectifier removed from the circuit, and (2) η_{DC-DC},

TABLE VII
RC VALUES FOR CEFI APPROXIMATION

R_p	R_1	R_3	R_5	R_7	R_9	C_2	C_4	C_6	C_8	C_{10}
8.2 kΩ	6 mΩ	26.5 Ω	177 Ω	628 Ω	1.93 kΩ	143.7 nF	7.75 nF	5.01 nF	4.07 nF	4.07 nF

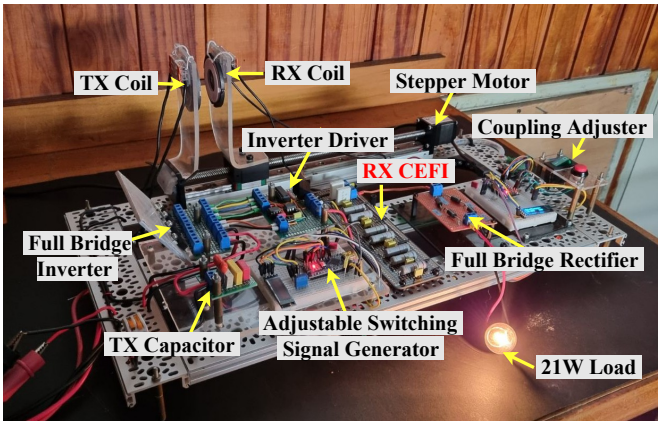

Fig. 10. Proposed fWPT experimental setup

TABLE VIII
COUPLING FACTOR AND DISTANCE RANGE FOR CWPT AND FWPT

k	cWPT Range (mm)	fWPT Range (mm)
0.94 - 0.95	0 - 5.4	0 - 2.4
0.89	6.0 - 9.0	3.0 - 6.0
0.71 - 0.73	9.6 - 15.0	4.2 - 9.0
0.39	17.4 - 24.0	11.4 - 16.8

measurements were taken at the DC supply at the high-frequency inverter and at the load after the full-bridge rectifier. The full-bridge rectifier used in the DC measurements consists of a standard four-diode configuration paired with a carefully selected output capacitor to suppress voltage ripple and ensure accurate power measurement. All AC waveform measurements in the experimental configurations were taken in RMS format, as required by the high-frequency operation of the system. A block diagram of the overall hardware system is presented in Figure 5. Two configurations were tested: (1) cWPT - classical wireless power transfer system using a standard capacitor and (2) fWPT - proposed system using a synthesised CEFI. Both systems were evaluated under identical conditions over a range of coupling coefficients ($0.3 \leq k \leq 0.95$).

V. EXPERIMENTAL RESULTS

This section presents the experimental results used to validate the theoretical model and simulation outcomes discussed in Section III-C. Figure 11 shows the input power requirements in different coupling coefficients for all four configurations of the system. Notably, at lower coupling coefficients ($k \leq 0.5$), all systems exhibit higher input power demands due to weak magnetic coupling and significant reflected impedance. However, the fWPT system consistently requires higher input power across all values of k, which can be attributed to its increased power handling capability enabled by the fractional capacitor. Unlike the classical capacitor, the CEFI modifies the impedance profile of the receiving side, allowing more power to be drawn and transferred even at moderate coupling levels.

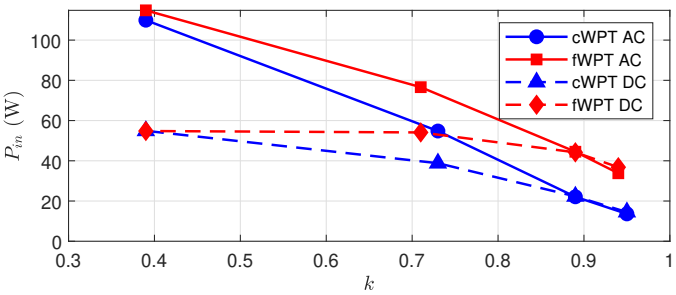

Fig. 11. Input power demand of the cWPT and fWPT systems

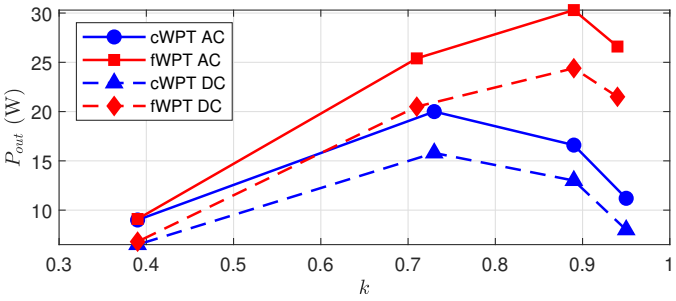

Fig. 12. Achieved output power of the cWPT and fWPT systems

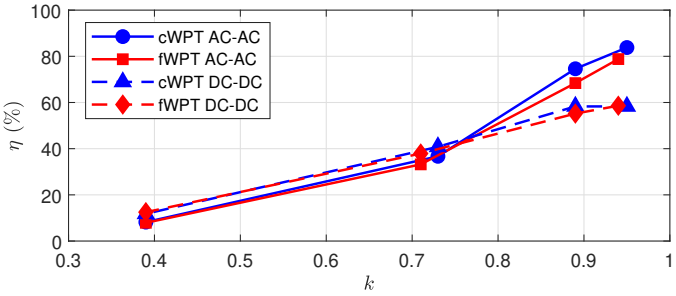

Fig. 13. Comparison of achieved system efficiencies

Figure 14 shows the output power, quantifying the relative performance improvement of the use of the fractional capacitor. The fWPT system significantly outperforms the cWPT configuration at all coupling levels, with the margin widening as k increases. This performance gain is a direct result of the sub-unity fractional impedance ($\alpha = 0.98$), which improves

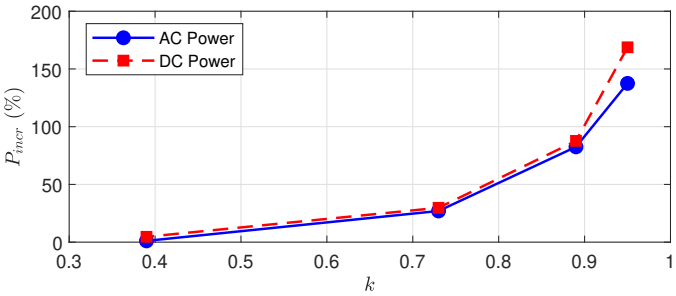

Fig. 14. Comparison of power outputs

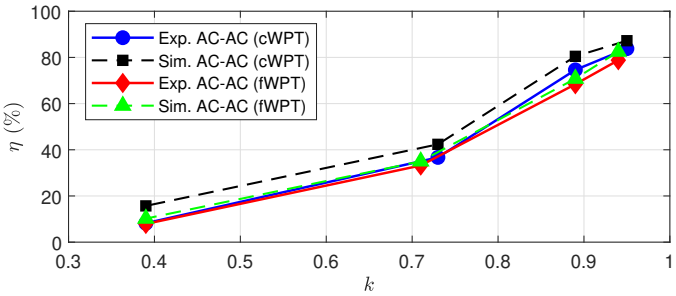

Fig. 15. Theoretical model-to-hardware agreement

TABLE IX
SUMMARY OF S-S WPT SYSTEMS

k_{avg}	System	DC P_{in} (W)	AC P_{in} (W)	AC P_{out} (W)	DC P_{out} (W)	AC-AC η (%)	DC-DC η (%)
0.95	cWPT	14.5	13.6	11.2	8.0	83.8	58.3
0.94	fWPT	36.8	33.8	26.6	21.5	78.8	58.6
Difference		+154%	+149%	+137%	+169%	-5.0	+0.3
0.89	cWPT	22.3	22.1	16.6	13.0	74.6	58.3
0.89	fWPT	44.2	44.5	30.3	24.4	68.4	55.2
Difference		+98.2%	+101%	+82.5%	+87.7%	-6.2	-3.1
0.73	cWPT	38.8	54.8	20.0	15.8	36.7	40.8
0.71	fWPT	54.1	76.6	25.4	20.5	33.2	37.9
Difference		+39.4%	+39.8%	+27%	+29.7%	-3.5	-2.9
0.39	cWPT	54.9	109.9	9.0	6.5	8.2	11.8
0.39	fWPT	54.8	114.8	9.1	6.8	7.9	12.5
Difference		-0.2%	+4.5%	+1.1%	+4.6%	-0.3	+0.7

voltage-current phase alignment and optimises power transfer conditions. The impedance seen by the load is effectively shifted toward the optimal load impedance Z_{opt}, as predicted by (8), resulting in higher usable power at the output. Table IX contains a summary of the measurements recorded and is ideal for a statistical comparison of the fWPT and cWPT configurations. Figure 13 presents the efficiency achieved by each system. While the cWPT system shows slightly higher AC-AC efficiency at high coupling (e.g., 83.8% at $k = 0.95$ vs. 78.8% for fWPT), this difference remains within an acceptable range (5%). Interestingly, the DC-DC efficiency remains nearly identical (58%) between both systems at high coupling. This suggests that although fWPT draws more power and delivers more output, it manages to do so without introducing significant additional losses, indicating well-matched system impedance and effective energy utilisation.

Figure 14 quantifies the performance improvements in percentage, denoted by P_{incr}, of the fWPT over the cWPT system. At $k = 0.95$, DC output power improves by 169% (21.5 W vs. 8.0 W), and AC power by 137% (26.6 W vs. 11.2 W). These results confirm the theoretical expectations: as $\alpha \leq 1$, the fractional element behaves like a "soft" reactive component that introduces favourable phase shift and energy storage dynamics, improving both voltage gain and power transfer. The improvement diminishes as k decreases due to the dominance of misalignment and resistive losses, but remains positive even in the low-coupling regime.

Collectively, these figures substantiate the claim that fractional-order capacitive elements, when properly designed and synthesised, can significantly enhance the power transfer capability of MRC-based WPT systems without incurring major efficiency penalties. This makes the proposed fWPT system particularly advantageous in applications requiring high-power delivery over short to moderate distances, such as EV charging stations or industrial automation platforms.

To show how the theoretical fWPT model aligns more closely with the practical model, a circuit simulation, matching the test conditions was conducted using Simscape© Electrical in Simulink©. The efficiency curves in Figure 15 were obtained after simulating the system at the same four k values.

While both approaches show increasing efficiency with coupling coefficient, the fWPT system demonstrates notably better agreement between experimental and simulated results. In contrast, the cWPT system shows a more pronounced discrepancy between simulation and experimental data, particularly at lower coupling coefficients.

VI. DISCUSSION

A. Advantages

(1) The experimental results demonstrate significant practical implications for the cWPT system. Using the proposed fractional-order circuit, an almost 169% increase in DC power output while maintaining comparable DC-DC efficiency. It represents a breakthrough for high-power, short-distance applications. This performance is particularly valuable for EV charging, where the improved power output could reduce charging times while maintaining efficiency, especially in stationary charging stations where coupling can be optimised.

(2) For real-world applications, when high-power wireless charging is demanded, such circuits can benefit from increased power capability without significant infrastructure modifications.

(3) Fast-charging consumer electronics, where devices can be precisely positioned, could leverage high efficiency and power output.

B. Limitations

(1) FOEs should demonstrate a constant phase angle within a specified frequency range called the constant phase zone.

Although the phase shift remains constant, the impedance of FOEs varies with frequency, thereby causing the conventional capacitance or inductance to change accordingly. These distinctive characteristics, while offering advantages over integer components, make the realisation process intricate and challenging, which explains why FOEs have not yet become commercially available products.

(2) The network synthesis approximation technique yields a fixed network structure, offering little flexibility if the system parameters are changed. Consequently, the designed EFI becomes specific to its intended system and purpose, lacking flexibility.

VII. Conclusion

This paper comprehensively investigated a novel WPT system that incorporated a passive CEFI in the receiving circuit. The theoretical framework was systematically validated in simulations, which demonstrated strong agreement between predicted and simulated performances for the fWPT system. In particular, our designed CEFI led to a two-fold increase in the optimal load value, from 4Ω to 8.2Ω at $k = 0.5$. This demonstrates a significant improvement in power handling capabilities. The experiment showed a 169% increase in DC power output and a 137% improvement in AC power output at $k = 0.95$. The close alignment between theoretical, simulation, and experimental results depicted the accuracy of the fractional analytical model for the fWPT. It showed better agreement compared to the cWPT system across all coupling coefficients. The result was promising for high-power and short-distance applications such as EV charging and industrial automation. The findings also conclude that passive CEFIs can play a crucial role in enhancing the performance of the WPT system, especially in scenarios where maximum power transfer takes priority over peak efficiency.

References

[1] A. Kurs, A. Karalis, R. Moffatt, J. Joannopoulos, P. Fisher, and M. Soljacic, "Wireless power transfer via strongly coupled magnetic resonances," *Science (New York, N.Y.)*, vol. 317, DOI 10.1126/science.1143254, pp. 83–6, 08 2007.

[2] G. Zhang, Z. Ou, and L. Qu, "A Fractional-Order Element (FOE)-Based Approach to Wireless Power Transmission for Frequency Reduction and Output Power Quality Improvement," *Electronics*, vol. 8, DOI 10.3390/electronics8091029, 09 2019.

[3] C. Rong, B. Zhang, Y. Jiang, X. Shu, and Z. Wei, "A misalignment-tolerant fractional-order wireless charging system with constant current or voltage output," *IEEE Transactions on Power Electronics*, vol. 37, DOI 10.1109/TPEL.2022.3164069, pp. 1–1, 09 2022.

[4] Y. Jiang and B. Zhang, "A fractional-order wireless power transfer system insensitive to resonant frequency," *IEEE Transactions on Power Electronics*, vol. PP, DOI 10.1109/TPEL.2019.2946964, pp. 1–1, 10 2020.

[5] D. A. Fathi, M. E. Fouda, L. A. Said, N. R. Khafagy, and A. G. Radwan, "Two-port network analysis of equal fractional-order wireless power transfer circuit," in *2020 32nd International Conference on Microelectronics (ICM)*, DOI 10.1109/icm50269.2020.9331780, pp. 1–4. IEEE, Dec. 2020. [Online]. Available: http://dx.doi.org/10.1109/ICM50269.2020.9331780

[6] R. Prasad, K. Sharma, B. Gulabdas, and U. Mehta, "Model of fractional-order resonant wireless power transfer system for optimal output," *Journal of Electrical Engineering*, vol. 73, DOI 10.2478/jee-2022-0034, pp. 258–266, 09 2022.

[7] A. Ali and U. Mehta, "A comprehensive review of wireless power transfer systems: Focused study with fractionalâorder elements," *International Journal of Circuit Theory and Applications*, DOI 10.1002/cta.3921, Jan. 2024. [Online]. Available: http://dx.doi.org/10.1002/cta.3921

[8] A. Ali and U. Mehta, "Performance analysis of fractional wireless power transfer systems via scattering parameters," in *2025 IEEE International Students' Conference on Electrical, Electronics and Computer Science (SCEECS)*, DOI 10.1109/SCEECS64059.2025.10940695, pp. 1–6, 2025.

[9] K. Kothari, U. Mehta, and R. Prasad, "Fractional-order system modeling and its applications," *Journal of Engineering Science and Technology Review*, vol. 12, no. 6, pp. 1–10, 2019.

[10] E. Piotrowska and K. Rogowski, "Time-domain analysis of fractional electrical circuit containing two ladder elements," *Electronics*, vol. 10, DOI 10.3390/electronics10040475, no. 4, 2021.

[11] R. Prasad, K. Kothari, and U. Mehta, "Flexible fractional supercapacitor model analyzed in time domain," *IEEE Access*, vol. 7, DOI 10.1109/ACCESS.2019.2938543, pp. 122 626–122 633, 2019.

[12] S. M. Abdelhafiz, M. E. Fouda, L. A. Said, and A. G. Radwan, "On fractional-order capacitive wireless power transfer system," in *2022 International Conference on Microelectronics (ICM)*, DOI 10.1109/ICM56065.2022.10005415, pp. 113–116, 2022.

[13] K. K. Gautam, A. Chatterjee, S. B. Santra, and D. Prasad, "Size Optimized Load Independent Constant Current and Constant Voltage Wireless Charging System for EVs," *IEEE Journal of Emerging and Selected Topics in Industrial Electronics*, DOI 10.1109/JESTIE.2025.3550840, pp. 1–11, 2025.

[14] C. Liu, W. Han, G. Yan, B. Zhang, and C. Li, "Receiver resonant frequency adaptive-tracking in wireless power transfer systems using primary variable capacitors," *IEEE Journal of Emerging and Selected Topics in Industrial Electronics*, DOI 10.1109/JESTIE.2025.3586663, pp. 1–9, 2025.

[15] W. Wang, K. Li, M. Duan, C. Xu, and Z. Lu, "Research on Power Supply Strategy of Multi-Battery Load WPTS3 Based on Tower Insulator," *IEEE Journal of Emerging and Selected Topics in Industrial Electronics*, DOI 10.1109/JESTIE.2025.3561460, pp. 1–12, 2025.

[16] Y. Jiang, B. Zhang, and J. Zhou, "A fractional-order resonant wireless power transfer system with inherently constant current output," *IEEE Access*, vol. PP, DOI 10.1109/ACCESS.2020.2970199, pp. 1–1, 01 2020.

[17] C. Rong, B. Zhang, and Y. Jiang, "Analysis of a fractional-order wireless power transfer system," *IEEE Transactions on Circuits and Systems II: Express Briefs*, vol. 67, DOI 10.1109/tcsii.2019.2949371, no. 10, pp. 1755–1759, Oct. 2020. [Online]. Available: http://dx.doi.org/10.1109/TCSII.2019.2949371

[18] T. Ohira, "The kQ Product as Viewed by an Analog Circuit Engineer," *IEEE Circuits and Systems Magazine*, vol. 17, DOI 10.1109/mcas.2016.2642698, no. 1, pp. 27–32, 2017. [Online]. Available: http://dx.doi.org/10.1109/MCAS.2016.2642698

[19] Y. Narusue, Y. Kawahara, and H. Morikawa, "Load optimization factors for analyzing the efficiency of wireless power transfer systems using two-port network parameters," *IEICE Electronics Express*, vol. 17, DOI 10.1587/elex.17.20200093, no. 10, p. , May. 2020.

[20] J. Hantschel, "Wireless energy transmission coils as key components," WÃ¼rth Elektronik eiSos GmbH Co. KG, Tech. Rep., 2013.

[21] N. Mijat, D. Jurisic, and G. S. Moschytz, "Analog modeling of fractional-order elements: A classical circuit theory approach," *IEEE Access*, vol. 9, DOI 10.1109/ACCESS.2021.3101160, pp. 110 309–110 331, 2021.

[22] A. Ali, A. Kumar, U. Mehta, and M. Cirrincione, *Intelligent data-driven approach for fractional-order wireless power transfer system*, pp. 218–236. CRC Press, Mar. 2024.

[23] D. Jurisic, N. Mijat, and G. S. Moschytz, "Matlab code for calculating the minimax immitance for approximating fractional-order elements," https://www.mathworks.com/matlabcentral/fileexchange/96762-fractional-order-elements-foes-using-minimax-approximation., accessed: 2023-08-17.

ARSHAQUE A. ALI (Graduate Student Member, IEEE) earned his BEng degree in electrical and electronics from The University of the South Pacific (USP), Fiji, in 2023. Currently, he is pursuing his MSc in Engineering at USP, where his research interests revolve around utilising fractional theory to design fractional components, with a primary focus on optimising wireless power transfer. His other research interests also include machine learning, power electronics, and embedded systems. He was a recipient of the National Toppers Scholarship (NTS) for his undergraduate studies. Moreover, he was awarded the gold medal for his outstanding performance in the electrical and electronics programme during his bachelor's studies and the Pacific Scholarship for Excellence in Research and Innovation (PSERI) for his graduate studies.

UTKAL MEHTA is a Senior Member of IEEE, having received the PhD degree in the area of system modelling and control from IIT Guwahati, India. Currently, Dr Mehta works in Electrical and Electronic Engineering at the University of the South Pacific, Fiji Islands. He worked as a project engineer (R&D) at Comp Power Corporation, USA. His research interests include power system control, modelling, applied fractional calculus, robotics applications for agriculture and industrial automation. He is leading the FraCAL Research Group at USP. He is an active volunteer of IEEE, contributing to several technical and professional activities within the Association.